Effects of Internal Cavitation on Breakup of High-Pressure Diesel Sprays

K.-S. Im[1], S.-K. Cheong[2], Christopher F. Powell[2], M-C Lai[3], and Jin Wang[*2]

[1] Livermore Software Technology Corp.
Livermore, CA 94551 USA

[2] Argonne National Laboratory
Argonne, IL 60439 USA

[3] Wayne State University
Detroit, MI 48202 USA

Abstract

Breakup process of liquid jets is complex and can be influenced by a large number of parameters including the details of the design of the injector, internal cavitation, flow turbulence, and the physical and thermodynamic states of both liquid and gas. For high-pressure diesel injection systems, the internal orifice geometry of injector nozzle can have a determining influence on earlier breakup and overall spray atomization, which is due to possible cavitation inside the nozzle. To understand the breakup phenomenon with the diesel injection and breakup, time-resolved x-radiography was employed to measure fuel mass distributions in the near-nozzle region of sprays for two simple single-orifice mini-sac nozzles. One has a hydroground orifice inlet, the other one was not subjected to the hydro-grinding process, which has sharp inlet edges. The injection was performed at 1000 bar of injection pressure to a spray chamber was filled with 1 atm helium gas at room temperature. For sprays with short injection duration, the spray cone angles were directly correlated with and dictated by the transient pintle motion in the injection nozzles. With longer injection duration (1 ms), drastically different cone angles were observed for the sprays from the two nozzles in the near-nozzle region (< 5 mm from the orifice exit). Most importantly, a 3D transient simulation of the nozzle internal flow with cavitation models was carried out using CFD techniques. The result has demonstrated that liquid-fuel breakup is extremely sensitive to nozzle internal geometry, especially, at a quasi-steady condition when the injector pintle is fully opened. We can attribute the different spray cone angles to the internal-cavitation-induced jet breakup, clearly demonstrated by numerical simulations of the internal cavitation flows by using the homogeneous equilibrium model.

Introduction

The instability and disintegration of liquid jets has been of theoretical and experimental interest for more than one hundred years because of its technological significance [1].

Recent advanced challenges in diesel engine technologies have employed increasingly high injection pressures (up to 200 MPa), smaller orifice diameters (less than 100 μm), and ultra transient (less than 500 μs duration) multiple injections for achieving better atomization of the fuel sprays. These requirements have brought greater impetus to the understanding of fluid dynamics of the flow inside the nozzle orifice and the fuel sprays immediately outside the nozzle exit, and their dependence on the nozzle geometry, for example the qualitative and quantitative investigation between the nozzle geometry and breakup characteristics [2-4].

For high-pressure, high-speed injection such as modern diesel engine, there are many proposed breakup mechanisms including turbulences of internal flows, spatial gradient and temporal pulsation of nozzle internal pressure, internal cavitation due to nozzle physical geometry, and change of velocity profile at the nozzle exit [5-7]. Spray phenomena near nozzle exit are of paramount crucial for verifying the theoretical speculations on jet breakup. However, the near-nozzle region has been difficult, if not impossible, to study due to its optical opacity caused by a large amount of small liquid droplets surrounding the jets.

Recently, a time-resolved, synchrotron-based x-ray absorption technique has been developed for probing the diesel fuel distribution quantitatively outside the injector orifices with a μs-temporal resolution [8-10]. Their results have provided quantitatively detailed structural and dynamical information for high pressure fuel sprays in the optically dense near-nozzle region. Such structural and dynamical properties of the fuel sprays are closely related to the

[*] wangj@aps.anl.gov

nozzle orifice geometry and structure on a μm-length scale, and the microstructure-induced fluid dynamics, such as cavitation and turbulence, inside the orifice.

Therefore, an interrogation of the entire injection process is required to understand the fuel-spray phenomena both outside and inside an injection orifice. Although most studies have been done primarily with scaled-up nozzles or transparent nozzles made of non-metal materials [11], the direct evidence to link the nozzle geometry and the spray dynamics for real injection nozzles has not been fully established. In addition, a previous attempt to identify the nozzle geometry effects on the spray characteristics was not effective [12] because the measurement was performed under injection conditions not appropriate to reveal the realistic injection effects.

The aim for the present study is to illustrate the influence of nozzle geometry on the properties of high-pressure, high-speed spray in an unambiguous manner by using the synchrotron x-ray-based radiographic technique and is to develop a numerical simulation technique for internal flows conjunction with modern cavitation models in realistic production nozzle geometry so as to better understanding the experiment results achieved and to predict the nozzle-geometry dependence of the near-nozzle spray behaviors.

Experimental Results

It has been speculated that the liquid breakup during high-pressure injection can be caused by the turbulence, cavitaion inside of the nozzle flow, and ambient aerodynamics outside of the nozzle. To illustrate the sole effect of the nozzle geometry, we chose two nominally axial-symmetric, single-orifice nozzles with a fine but distinctive feature difference: one has a hydroground orifice inlet and the other does not as shown schematically in Figure 1.

To obtain the sole effects of nozzle geometry on the near-nozzle jet breakup, we used the following testing conditions: 1) The injection was performed into a spray chamber filled with helium gas at 1 bar pressure and at room temperature (typically 25-28°C). Helium, the lightest inert gas with molecular weight of 4, was used to reduce the aerodynamics-assisted fuel breakup [13, 14] and 2) The nominal injection time was chosen from 400 to 1 ms. With the longer injection time (1 ms), a quasi-steady flow can be established, free of the effect of the pintle motion, within a large fraction of the injection duration. The radiographic images of the sprays were collected by a focused and monochromatic synchrotron x-ray beam, 8 keV, 200 (H) x 30 (V) μm^2, at the XOR 1-BM beamline of the Advanced Photon Source (APS), in conjunction with a fast avalanche photodiode (APD) point detector [10]. The data were collected by positioning the transient fuel spray between the x-ray beam and an APD and recording the time-resolved response of the detector on a transient digitizing oscilloscope. For single-wavelength x-rays transmitting through a nonuniformly distributed material (fuel jet), the analysis of the fuel mass (M) in the beam from measured x-ray transmission (I/I_0) and the fuel mass absorption coefficient (μ_M) of the attenuating material is straightforward, as

$$M = -\frac{1}{\mu_M}\ln\left(\frac{I}{I_0}\right). \qquad (1)$$

Thus, the time evolution of the measured x-ray transmission can be simply transformed into integrated, line-of-sight mass data at each point in the image of the fuel spray.

Figure2 illustrated the spray cone angle can be determined by measuring the absolute fuel distribution (2D, line-of-sight projection) in the radial direction of the spray. The spray was generated with 1000-bar injection pressure and the injection time of 400 μs using the hydroground nozzle. The full-width-at-half-maximum (FWHM) of the fuel mass distribution at various positions (0.2, 3.2, and 5.2 mm from the nozzle exit, marked as dashed lines) was measured at specific time instances, 120, 330, and 480 μs from the start of injection (SOI). The microscopic half cone angles are shown in each of the lower panels: 2.39° at 120 μs, 0.24° at 330 μs, and 1.24° at 480 μs after SOI, as also shown in Figure 2. It is obvious that the cone angle is significantly affected by the time after SOI and, more fundamentally, by the transient state of the needle.

For the nonhydroground nozzle, we also observed time-dependent microscopic spray cone angle changes in Figure 3. Although the cone angles are slightly bigger than those of the hydroground case, the temporal variations are similar to the hydroground case.

When a longer injection time (1 ms) was used, the spray behavior became distinctively different between two nozzles. Figure 4 shows snapshots of the sprays injected also at 1000 bar to helium gas. During the pintle opening process, larger spray cone angles are present (Figures 4a and 4f), similar to those seen in the 400-μs-injection-time case (Figure 2a) for both nozzles. After the nozzle is fully opened at 500 μs after SOI, the spray patterns are drastically different. For sprays from the hydroground nozzle, the spray cone angle approaches 0° showing as a steady jet with minimum breakup (Figures 4b – 4d). During the same time, the spray from the nonhydroground nozzle is also steady, but the liquid breakup is apparent as indicated by the finite spray angles (Figures 4g – 4i). In both cases, the cone angle stays as a constant until the pintle starts to close. The cone angles increase near the end of the injection

(Figures 4e and 4j, more obvious in Figure 4e) to a value similar to that in the short-injection case (as shown in Figure 3), a signature of the pintle-motion-induced breakup.

To clearly summarize the observation, the time-dependent microscopic spray cone angles are plotted in Figure 5. Here, the evolution of the cone angle data is dramatically different for the two nozzles. In the steady flow, for the nonhydroground nozzle, the spray cone angle never diminishes to 0°. Rather, it keeps a steady value of about 4°, which is comparable to the angles during the pintle opening and closing periods.

To further illustrate the fuel mass distribution in the sprays, we performed a model-dependent three-dimensional (3D) reconstruction using the line-of-sight radiography data shown in Figure 6. The models consist of a single assumption: the distribution has either circular or elliptical cross-sectional distribution. We note that the specific gravity of the diesel calibration fluid (with Ce-containing additives) was measured to be 880 $\mu g/mm^3$. The volume fraction of fuel (either in the liquid or gas form) is close to unity for the hydroground nozzle at the center of the spray core.

Not surprisingly, the fuel mass density behaves quite differently in the case of the nonhydroground nozzles. Instead of having a high-density jet, the spray spreads in the radial direction, and its mass density decreases rapidly along the spray axis, as shown in Figure 7. At 3 mm from the orifice exit, the maximum on-axis fuel density drops to a value equivalent to a volume fraction of about 25%.

Numerical Simulation

The difference in near-nozzles sprays is so distinctive that it must be due to the different behaviors of liquid flow and breakup inside the orifice. It is extremely difficult, if not impossible, to directly observe the highly transient internal nozzle cavitating flow because of the small size of the nozzle orifice and high-speed flow in such a nontransparent enclosure. Therefore, we resorted to numerical simulation to shed more light to understand this problem. The numerical simulation of cavitating internal nozzle flows in high-pressure, high-speed diesel injectors has become a widely interested topic because the cavitation phenomenon inside a fuel nozzle injector can provide valuable and detailed information for nozzle design and spray breakup modeling. Many studies have tried to predict complex cavitating flows by numerical methods. Among the existing methods, we applied Schmidt's homogeneous equilibrium model [15], which is based on the acoustic speed of the mixture of liquid and vapor. This model is simple but contains the important characteristic information of cavitating flows. More specifically, for present diesel injection systems like a small geometry (180 μm of nozzle diameter) and very high velocities (driven by 1000-bar injection pressure through the nozzle), the continuum model considering the compressibility of the liquid and vapor should be able to correctly predict the cavitaing effects due to the two different nozzle geometries, which ultimately induced distinctively different the sprays so that our simulation would be able capture the essential internal flow and cavitation characteristics for understanding the near-nozzle breakup due to in-nozzle cavitation.

The computational meshes, shown in Figure 8, simulate two different internal geometries of the two single-orifice nozzles illustrated in Figure 2. Total cell numbers in the calculation were about 62000 for the nonhydroground and the hydroground nozzle. Since cavitating flows are generally highly transient and in multiple phases, the numerical method should be time-accurate and robust to accommodate complex cavitation models. In this study we use the space-time conservation element and solution element (CE/SE) method by Chang [16]. We remark that the CE/SE method is substantially different in both concept and methodology from the traditional computational fluid dynamics (CFD) methods.

To provide a crucial evidence for distinctive spray cone angles in a semi-steady flow during long injection duration, the calculation starting with ambient condition inside nozzle was continued until the flow was reached steady-state. Figure 9 shows a snapshot of internal cavitating flows for different geometries. As we expected, the nonhydroground nozzle generates very strong cavitations while the hydroground generates only weak cavitating flow so that it is obvious to see the main differences influenced by geometrical differences.

To further illustrate the geometrical effect on the generation of distinctive spray cone angles between the hydroground and nondydroground geometries, the velocity components both in axial direction (u_x) and in the perpendicular direction (u_y) were integrated and taken the average value along axial position in the orifice, x/D, where D is nozzle diameter. The ratio between u_x and u_y, characterizing the averaged flow divergent angle due to the cavitation are plotted in c) and d) at close to the exit of the orifice (x/D =3.5 to 4.5 from nozzle inlet). The essential features of cavitating flows are liquid/vapor phase change, high gradients of flow variables, and unsteadiness. Whenever cavitation takes place inside a nozzle orifice, a cavitation cloud is always observed downstream of the cavity [17] and there is a strong interaction between the cavitation cloud and large-scale vortices, leading to the formation of vortex cavitation (see also in Figure 9a). In the case of hydroground nozzle, the change of the velocity direction is not enough to generate strong cavitation in the downstream. Once the cavitation is generated in the nonhydroground nozzle, it grows and interacts with each other, and also transferring mass, momentum, and heat with liquid, making

the physical processes extremely unstable and complex as expected. Therefore, we strongly believe that the cavitation is the main source to change the spray shape drastically different.

Discussion

Although the above quantitative 3D tomographic-type reconstruction based on x-ray radiograph provides the spray mass distribution, the data do not resolved direct spray morphology for understanding the spray cone angle difference for the two nozzles. The small cone angles in the case of the hydroground nozzle can be attributed to the material reduction at the ambient gas/liquid interface even in the light-density surrounding gas–helium. Liquid could be peeled off from the jet as a result of primary breakup, resulting in a thinner liquid jet along the jet axis. This argument can be tested with further analysis of the quantitative x-ray radiographic images obtained in this measurement. At the quasi-steady condition, e.g., at the 750-μs time instance during the 1-ms injection process, the fuel mass integrated in the planes perpendicular to the spray axis will yield the linear fuel density in the spray. If the injection is steady, the spray velocity should be relatively constant within the first several millimeters from the orifice exit to maintain the conservation of the fuel mass flux if all the spray mass is accounted for by the x-ray measurement. If the jet is evaporative or the liquid breakup is strong, this mass-flux conservation can be verified by this experiment due to the fact that x-rays are not very sensitive to small liquid droplets and fuel vapor. Figure 10 shows the so-integrated linear mass density distribution along the spray axis for both nozzles at 750 μs after SOI. Indeed, for both cases, the density distribution is close to constant, indicating that the mass flux is conserved. Therefore, all the fuel mass has been accounted for in the measurement and the measurement reveals the fuel mass distribution truthfully.

We can now be confident that this measurement of spray mass distribution and spray cone angles is reliable and can be used to understand the correlation between the nozzle geometry and the spray behaviors. It is well known that cavitation in injection nozzles has a strong impact on liquid jet breakup and spray formation. However, it is difficult, at least for now, to directly visualize the cavitation inside actual high-pressure injection nozzles such as the ones used in this experiment. As a result, numerical simulation is a necessary and powerful tool to provide a better understanding of the cavitating flows. Since the vertical component of the internal-flow velocity is small compared to its axial component in the orifice, the near-nozzle spray angle can be inferred by the computed maximum ratio of the vertical velocity to the axial component at the nozzle exit [18]. The computed angle can be directly compared with the actual spray angle, measured by x-radiography and calculated based on the FWHM profile. The angles values agree quantitatively between the measured angle outside the nozzle and velocity angle immediately inside the nozzle exit. Even though our simulation results are strongly support to provide a crucial clue for the experimental observations, we currently are in the process of developing more advanced numerical simulation of full-scale 3D internal flows with realistic cavitation model and boundary conditions.

Conclusion

We used time-resolved x-radiography to measure the fuel mass distributions in the near-nozzle region of sprays from two single-orifice mini-sac nozzles with and without a hydroground orifice inlet. During a relatively long injection event (1 ms), we demonstrated drastically different cone angles for the sprays from the two nozzles in the near-nozzle region (< 5 mm from the orifice exit). This result strongly indicates that the liquid fuel breakup is extremely sensitive to the nozzle internal geometry, especially, at a quasi-steady condition when the injector pintle is fully opened. We attributed the different spray cone angles to internal-cavitation-induced jet breakup, as supported by a 3D numerical simulation of internal flow, where qualitative agreement between the experimental results and the simulation is demonstrated.

Acknowledgments

We thank J. Schaller for providing the nozzles. We are also grateful to the sponsorship of U.S. Department of Energy (DoE) FreedomCAR and Vehicle Technology Program. This work and the use of the APS are supported by the DoE, Office of Science, Office of Basic Energy Sciences, under contract No. DE-AC02-06CH11357.

References

1. Rayleigh, L., *Proc. London Math. Soc.* 10:4-13 (1878).
2. Chen, H.H., and Brenner, M.P., *Phys. Rev. Lett.* 92:166106(166104) (2004).
3. McCarthy, M.J., and Molloy, N.A., *Chem. Eng. J.* 7:1-20 (1974).
4. McGuinness, P., Drenckhan, W., and Weaire, D., J. *Phys. D: Appl. Phys.* 38:3382-3386 (2005).
5. Kaminoto, T., *Spray Formation and Combustion. In Advanced Combustion Science*, Someya, T., Ed. Springer-Verlag: Tokyo, 1993.
6. Reitz, R.D. *Atomization and Other Breakup Regimes of a Liquid Jet.* Princeton University, Princeton, NJ, 1978.

7. Rietz, R.D., *Atomisation Sprays Techology* 3:309-337 (1987).
8. Cai, W., Powell, C.F., Yue, Y., Narayanan, S., Wang, J., Tate, M.W., Renzi, M.J., Ercan, A., Fontes, E., and Gruner, S.M., *Appl. Phys. Lett*. 83:1671-1673 (2003).
9. MacPhee, A., Tate, M.W., Powell, C.F., Yue, Y., Renzi, M.J., Ercan, A., Narayanan, S., Fontes, E., Walter, J., Schaller, J., Gruner, S.M., and Wang, J., *Science* 295:1261-1263 (2002).
10. Powell, C.F., Yue, Y., Poola, R., and Wang, J., *J. Synchrotron Rad*. 7:356-360 (2000).
11. Blessing, M., König, G., Krüger, C., Michels, U., and Schwarz, V., *SAE Technical Paper* 2003-01-1358.
12. Powell, C.F., Ciatti, S.A., Cheong, S.-K., Liu, J., and Wang, J., *SAE Technical Paper* 2004-2001-2011.
13. Clark, C.J., and Dombrowski, N., *Pro. R. Soc. Lond. A.* 329:467-478 (1972).
14. Xu, L., Zhang, W.W., and Nagel, S.R., *Phys. Rev. Lett.* 94:184505(184504) (2005).
15. Schmidt, D.P.,*Rutland, C. J., Corradini, M. L., Atomisation Sprays Techology* 9:255-276 (1999).
16. Chang, S. C., *J of Comput. Phys.* 119:295-324 (1995).
17. Kubota, A, Kato, H, Yamaguchis, H, and Maeda, M., *J of Fluids Eng.* 11:204-210 (1989).
18. Schweitzer, P. H., *J. Appl. Phys.* 8, 513-521 (1937).

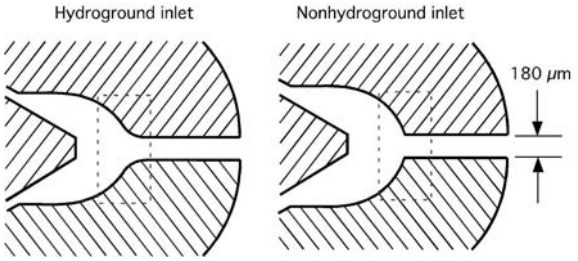

Figure 1. Schematics of two single-orifice nozzles used in the present study: with a hydroground inlet (left) and nonhydroground inlet (right), as highlighted in the dashed rectangles. The schematics are drawn approximately to scale. The pintle is illustrated at its open position.

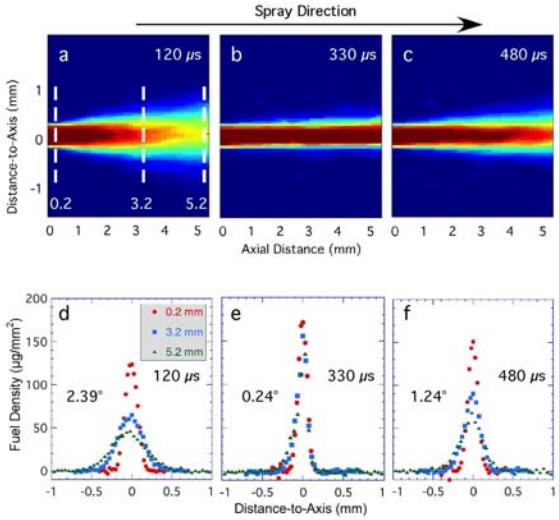

Figure 2. Microscopic cone angle measurement of the fuel sprays by x-radiography, with a short injection duration of nominal 400 μs from the hydroground nozzle into He gas, within 5.3 mm from the orifice exit at a) and d) 120 μs (during needle opening); b) and e) 330 μs (needle opened); and c) and f) 480 μs (during the needle closing). The upper panels (a-c) display the composite spray images and the lower ones (d-f) show the projected (line-of-sight integrated) fuel mass distribution at several axial locations highlighted by the dashed lines in a.

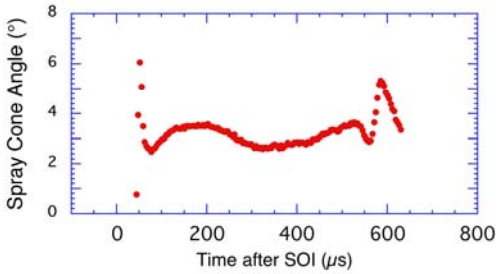

Figure 3. Time-dependent microscopic spray cone angle for the nonhydroground nozzle using the same injection and measurement conditions as in Figure 2.

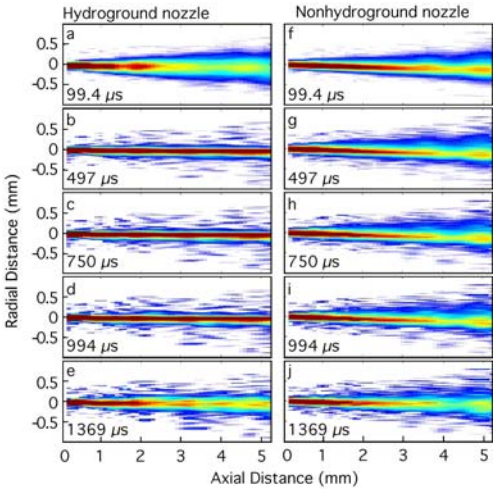

Figure 4 Snapshots of time-resolved radiographs of sprays from the hydroground and nonhydroground nozzles with 1-ms nominal injection time and at 1000-bar injection pressure.

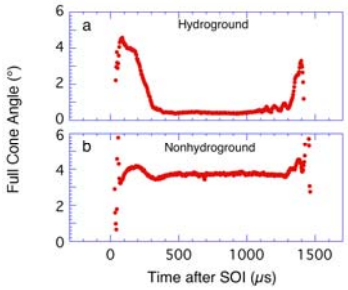

Figure 5. Time-dependent microscopic spray cone angles for the hydroground and nonhydroground nozzles with injection duration of 1 ms.

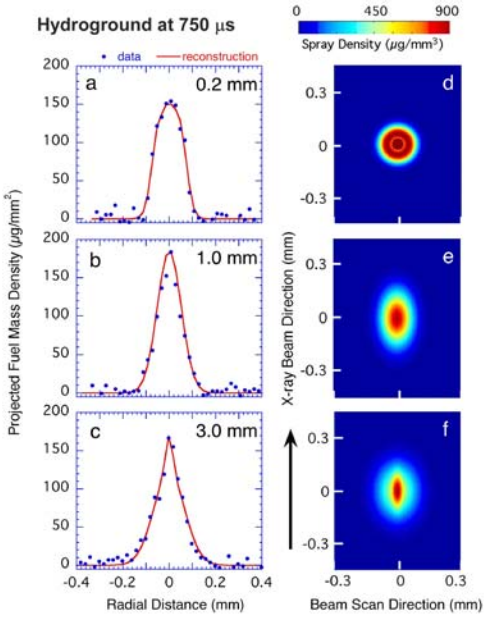

Figure 6. Projected fuel mass density along the direction of the x-ray beam (left panels) and the reconstructed 3D fuel density distribution (cross-sections at the corresponding axial distances, right panels) at 0.2 mm (a, d), 1.0 mm (b, e), and 3.0 mm (c, f) from the hydroground nozzle. Within the first 3 mm from the nozzle exit, although the jet cross-sectional shape can be distorted to elliptical form, the values of fuel volume fraction at the center of the spray core are all close to unity, corresponding to 880 μg/mm^3.

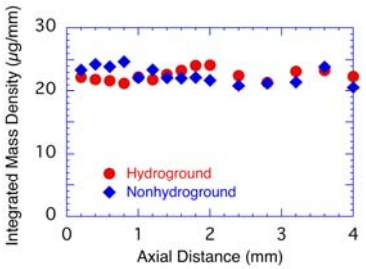

Figure 10. Integrated (linear) mass density distribution along the spray axis at 750 μs after SOI when the injections are in a quasi-steady state.

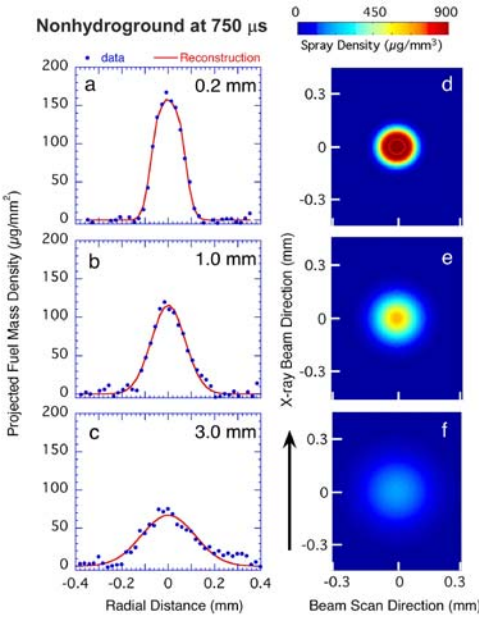

Figure 7. Projected fuel mass density along the direction of the x-ray beam (left panels) and the reconstructed 3D fuel density distribution (right panels) at 0.2 mm (a, d), 1.0 mm (b, e), and 3.0 mm (c, f) from the nonhydroground nozzle. The values of fuel volume fraction at the center of the spray core decreases dramatically along the spray axis.

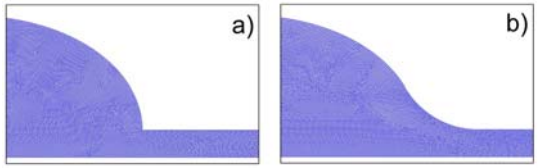

Figure 8. Schematics of the computational meshes for two single-orifice nozzles: a) nonhydroground inlet and b) hydroground inlet.

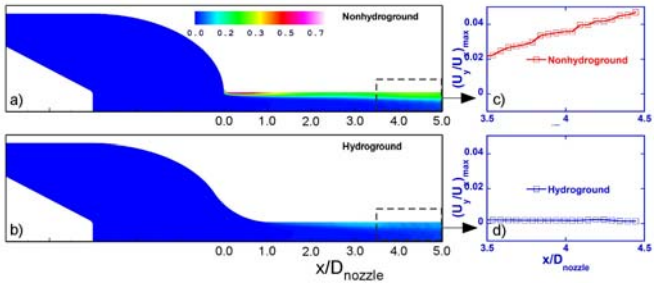

Figure 9. Comparisons of cavitating flows for nonhydroground inlet and hydroground inlet: a) and b). Velocity ratio comparisons in axial and perpendicular direction along axial position close to the exit of the orifice: c) and d). The coordinate origin is located at the inlet of the nozzle with a dimensionless variable x/D=0, using nozzle diameter D, and the nozzle exit is at x/D=5.